Raney Ni-Sn Catalyst for H_2 Production from Biomass-Derived Hydrocarbons

G. W. Huber, J. W. Shabaker, J. A. Dumesic*

Hydrogen (H_2) was produced by aqueous-phase reforming of biomass-derived oxygenated hydrocarbons at temperatures near 500 kelvin over a tin-promoted Raney-nickel catalyst. The performance of this non–precious metal catalyst compares favorably with that of platinum-based catalysts for production of hydrogen from ethylene glycol, glycerol, and sorbitol. The addition of tin to nickel decreases the rate of methane formation from C-O bond cleavage while maintaining the high rates of C-C bond cleavage required for hydrogen formation.

Hydrogen fuel cells are highly efficient devices for the production of electrical power, but it has recently been noted that "As yet, there is no energy- and cost-efficient method for making hydrogen, let alone burning it as a fuel" (*1*, p. 1686). Technologies exist for production of H_2 by steam reforming of nonrenewable fossil fuels (*2*); however, the full environmental benefit of moving toward a hydrogen society is realized only when H_2 is produced from renewable resources, such as water (by the action of sunlight) or biomass (by catalytic conversion). The effectiveness of biomass as a H_2 source depends critically on the discovery of new generations of heterogeneous (*3*, *4*), homogeneous (*5*), and/or enzyme catalysts (*6*). Such advances are of major importance for the catalytic production of H_2 from biomass, because this process is accompanied by the production of various by-products (*7*–*10*).

We have recently reported that it is possible to generate H_2 catalytically at mild reaction temperatures (e.g., 500 K) by aqueous-phase reforming of biomass-derived oxygenated hydrocarbons having a C:O stoichiometry of 1:1 (*7*). At the reaction temperatures of aqueous-phase reforming, however, the H_2 and CO_2 produced are thermodynamically unstable with respect to the formation of alkanes. Reaction kinetics studies for aqueous-phase reforming of ethylene glycol over various supported metals (*8*, *9*) indicate that Pt and Pd catalysts are selective for production of H_2, with Pt showing higher catalytic activity. Metals such as Ni and Ru exhibit good catalytic activity but lead to the formation of alkanes, whereas Rh, Ir, Co, Cu, Ag, Au, and Fe have low catalytic activity for aqueous-phase reforming reactions.

The high cost and limited availability of Pt make it advantageous to develop less expensive catalysts for our process based on non–precious metals. We have discovered a heterogeneous catalyst based on Ni, Sn, and Al that is both active and selective for the production of H_2 by aqueous-phase reforming of ethylene glycol, glycerol, and sorbitol. Sorbitol can be produced by hydrogenation of glucose (*11*), glycerol is a by-product in the production of biodiesel fuel from triglycerides (*12*), and glycerol and ethylene glycol can be produced from hydrogenolysis of sorbitol (*13*). This non–precious metal catalyst system was identified through a combination of fundamental and high-throughput studies, and this material shows catalytic activity, selectivity, and stability for H_2 production that are comparable to the performance of a Pt/Al_2O_3 catalyst (*7*).

The desired catalytic pathway for the production of H_2 and CO_2 by aqueous-phase reforming of oxygenated hydrocarbons involves cleavage of C-C bonds as well as C-H and/or O-H bonds to form adsorbed species on the catalyst surface (fig. S1). Cleavage of these bonds occurs readily over group VIII metals, such as Pd and Rh (*14*). Ethylene glycol and glycerol decompose on Pt to form adsorbed CO at room temperature (*15*, *16*). Adsorbed CO species must be removed from the surface by the water-gas shift reaction to form CO_2 and H_2, because high surface coverages by CO lead to low catalytic activity.

Undesired by-products may arise from parallel and series pathways (fig. S1). Parallel reactions proceed through cleavage of C-O bonds followed by hydrogenation to form alcohols or by rearrangement reactions to form organic acids. Series reactions arise from hydrogenation of adsorbed CO and CO_2 to form alkanes. Thus, a good catalyst for production of H_2 by aqueous-phase reforming must facilitate C-C bond cleavage and promote removal of adsorbed CO species by the water-gas shift reaction, but the catalyst must not facilitate C-O bond cleavage and hydrogenation of CO or CO_2.

Department of Chemical and Biological Engineering, University of Wisconsin, Madison, WI 53706, USA.

*To whom correspondence should be addressed. E-mail: dumesic@engr.wisc.edu

To aid our search for a non–precious metal catalyst that displays good activity and selectivity for H_2 production by aqueous-phase reforming, we developed a high-throughput, 48-well parallel batch reactor for catalyst screening (*17*). We tested more than 300 catalysts for aqueous-phase reforming of ethylene glycol, including monometallic catalysts, bimetallic catalysts, and metallic catalysts promoted with various metal oxides. Promising catalysts from high-throughput screening tests were subsequently studied in a bench-scale, aqueous-phase reforming flow reactor (*17*). Using this approach, we found that the addition of Sn to Raney-Ni catalysts significantly decreased the rate of methane formation without inhibiting the rate of H_2 production (fig. S2 and table S1). The optimal Sn-promoted Raney-Ni catalyst was prepared by decomposition of tributyl tin acetate (*17*) and had a bulk Sn/Ni atomic ratio of 0.075.

Table 1 shows experimental results for aqueous-phase reforming of sorbitol, glycerol, and ethylene glycol over Raney-NiSn. The gas-phase products were 50 to 70 mole percent (mol%) H_2, 30 to 40 mol% CO_2, and 2 to 11 mol% alkanes. Small amounts of CO [$<$1000 parts per million (ppm)] were detected in the outlet gas stream. The liquid products contained small amounts of alcohols, organic acids, and aldehydes ($<$50 ppm at conversions of $>$90%), as determined by high-performance liquid chromatography and gas chromatography (*9*, *10*). Analyses of the effluent gas and liquid streams yielded a complete carbon balance for all feed molecules. The selectivity for production of H_2 decreased slightly as the concentration of the oxygenated hydrocarbon increased from 1 to 5 weight % (wt %). Catalytic activity measured at 498 K and conversions near 15% decreased by only 15% after 10 hours and reached a constant value equal to 72% of the initial activity after 48 hours.

Selectivities for production of H_2 and alkanes are shown versus the feed molecule and temperature in Fig. 1 for the Raney-NiSn and 3 wt % Pt/Al_2O_3 catalysts (*7*). The Raney-NiSn catalyst exhibited higher selectivity for production of H_2 and lower selectivity for production of alkanes than Pt/Al_2O_3 for reforming of glycerol and ethylene glycol solutions, especially at higher temperatures. Comparable selectivities were observed over the two catalysts when sorbitol was used as the feed molecule. The CO concentrations of the product gases for both catalysts were also comparable (100 to 1000 ppm). Elsewhere we discuss how the product CO concentration can be reduced to $<$100 ppm by using a second reactor (*18*). Over both catalysts, the selectivity for production of H_2 improves in the order sorbitol $<$ glycerol $<$ ethylene glycerol, whereas the selectivity for produc-

tion of alkanes follows the opposite trend. Lower operating temperatures resulted in higher selectivities for production of H_2 (Fig. 1), which may be due in part to lower conversions of the feed molecules.

The turnover frequencies (TOFs) for H_2 production at 498 K by aqueous-phase reforming of 5 wt % ethylene glycol solutions were 1.1, 1.4, and 5.3 min^{-1} with H_2 selectivities of 47, 93, and 98% for Raney-Ni, Raney-NiSn, and 3 wt % Pt/Al_2O_3, respectively (after 6 hours time on stream). These values have been normalized by the number of surface metal atoms, as counted by the irreversible extent of CO adsorption at 300 K (i.e., the amount of adsorbed CO that cannot be removed by evacuation). (To calculate TOFs normalized by saturation H_2 uptakes, we note that the surface CO:H ratios from the saturation uptakes of CO and H_2 at 300 K were 0.72, 4.14, and 0.73 for Raney-Ni, Raney-NiSn, and 3 wt % Pt/Al_2O_3, respectively.) The Raney-NiSn catalyst has 1.6 times as many surface sites per gram (on the basis of CO adsorption) and has a higher bed density than Pt/Al_2O_3 (i.e., 1.5 versus 0.8 g/cm^3). Thus, the rates of H_2 production per unit volume at 498 K are comparable over both catalysts, equal to 350 and 450 μmol H_2 per cm^3 reactor per minute for Raney-NiSn and Pt/Al_2O_3, respectively. Previously, we determined that the rate of H_2 production by aqueous-phase reforming was not strongly limited by transport phenomena over Pt/Al_2O_3 catalysts (*9*). Because the reaction rates per unit volume for Raney-NiSn and Pt/Al_2O_3 are similar, we conclude that the activity of Raney-NiSn is not highly controlled by transport limitations.

Addition of Sn to Raney-Ni and subsequent exposure of the catalyst to reaction conditions had no effect on the BET (Brunauer-Emmett-Teller) surface area (which ranged from 46.6 to 48.8 $m^2\ g^{-1}$) and x-ray diffraction (XRD) pattern of the catalyst. All XRD peaks observed for the Raney-Ni and Raney-NiSn catalysts before and after exposure to reaction conditions for 60 hours were metallic Ni peaks. The XRD peak widths were similar for all three catalysts, indicating that the Ni particle sizes (estimated to be ~40 nm from the Scherrer equation) were comparable.

Scanning electron microscopy (SEM) images of Raney-Ni before and after exposure to reaction conditions (Fig. 2A) showed two separate phases: a predominant porous region and a less extensive solid phase randomly distributed on top of the porous region. X-ray microanalyses of these two regions indicated that the porous region was Ni-rich and that the other region was rich in Al and O. These results are consistent with previous electron microscopy and electron diffraction studies, which concluded that Raney-Ni catalysts are porous Ni frameworks covered by hydrated alumina particles [mostly bayerite and gibbsite $Al(OH)_3$] (*19*). The Raney-NiSn catalyst before reaction (Fig. 2B) also appears to have two separate phases: a predominant porous region and a diffuse phase covering parts of the porous region. X-ray microanalyses could not differentiate between these two phases. After reaction, the diffuse phase disappeared and two separate phases were seen, both of which contain Sn: porous Ni-rich regions (Fig. 2C) and crystalline regions containing primarily Al and O (Fig. 2D). Thus, the Al-rich phase forms crystallites (100 to 700 nm long) after exposure to aqueous-phase reforming reaction conditions, whereas the porous Ni-rich region remains intact.

In situ ^{119}Sn Mössbauer spectroscopy was used to determine the chemical environment of the Sn species in Raney-NiSn before and after aqueous-phase reforming of ethylene glycol (Fig. 3). The reduced catalyst contains Sn in three states: Ni_3Sn, Ni_3Sn_4, and metallic Sn, with relative spectral areas of 64, 6, and 30%, respectively. After exposure to reaction conditions, the metallic Sn and Ni_3Sn_4 peaks disappeared and a Sn(IV) peak appeared. The relative areas of the Ni_3Sn and Sn(IV) peaks were 90 and 10%,

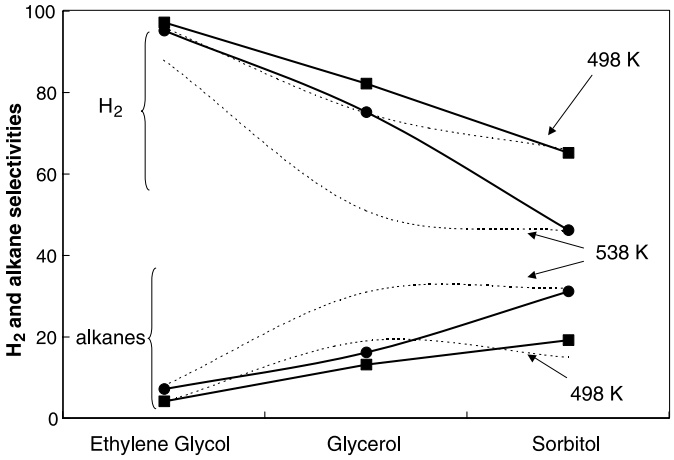

Fig. 1. Comparison of H_2 and alkane selectivities (%) of Raney-NiSn (squares and circles at 498 and 538 K, respectively) and 3 wt % Pt/Al_2O_3 (dashed lines) for aqueous-phase reforming of 1 wt % oxygenated hydrocarbons versus oxygenated hydrocarbon. High conversions (50 to 99%) of the reactants were achieved under these conditions, as reported in Table 1 and by Cortright *et al.* (*7*).

Table 1. Experimental data for reforming of oxygenated hydrocarbons over Raney-NiSn. H_2 selectivity (%) is calculated as (molecules H_2 produced/C atoms in gas phase)(1/*RR*) × 100, where *RR* is the H_2/CO_2 reforming ratio, which depends on the reactant compound. *RR* values for the compounds are as follows: sorbitol, 13/6; glycerol, 7/3; and ethylene glycol, 5/2. H_2 and alkane selectivities do not add up to 100% because they are based on independent H and C balances, respectively. Alkane selectivity (%) is calculated as (C atoms in gaseous alkanes/total C atoms in gas-phase product) × 100. The standard deviation in replicate gas or liquid analyses was ~2% of the average value reported below. The liquid hourly space velocity is defined as (volumetric feed flow rate)/(catalyst volume).

Conditions	Reactants											
	Sorbitol				Glycerol				Ethylene glycol			
Temperature (K)	498		538		498		538		498		538	
Pressure (bar)	25.8		51.4		25.8		51.4		25.8		51.4	
Feed concentration (wt %)	1	5	1	5	1	5	1	5	1	5	1	5
Liquid hourly space velocity ($hour^{-1}$)	1.64	0.82	1.64	1.64	1.64	0.82	10.3	1.64	5.14	2.57	12.9	10.3
Carbon in liquid-phase effluent (%)	44	39	9	27	13	22	4	3	2	4	0	6
Carbon in gas-phase effluent (%)	55	59	90	75	86	81	100	99	93	93	100	97
Gas-phase composition												
H_2 (mol%)	59	52	52	51	66	64	64	62	70	69	70	71
CO_2 (mol%)	34	39	36	38	30	32	30	31	28	28	28	27
CH_4 (mol%)	6.1	7.5	8.2	8.1	4.5	4.5	5.8	7.0	1.3	2.7	2.0	2.0
C_2H_6 (mol%)	0.8	1.2	2.1	2.1	0.0	0.1	0.1	0.5	0.0	0.1	0.0	0.1
C_3H_8 (mol%)	0.1	0.2	0.8	0.9	0.0	0.0	0.0	0.0	0.0	0.0	0.0	0.0
C_4, C_5, C_6 alkanes (mol%)	0.0	0.1	0.4	0.7	0.0	0.0	0.0	0.0	0.0	0.0	0.0	0.0
H_2 selectivity (%)	65	48	46	42	81	74	76	68	95	90	95	96
Alkane selectivity (%)	19	22	31	32	13	13	17	21	4	9	7	7

respectively. In view of the SEM results, it is probable that the Sn(IV) peak is associated with crystalline alumina. The Ni_3Sn alloy phase probably surrounds a phase that is Ni-rich (seen in XRD), because the Ni-Sn phase diagram predicts a mixture of Ni_3Sn and Ni for the overall composition of our Raney-NiSn catalyst (*20*).

Addition of Sn to the Raney-Ni catalyst decreased the irreversible extent of CO chemisorption from 220 to 170 μmol g^{-1}. The CO uptake decreased further to 140 μmol g^{-1} after exposure to reaction conditions, passivation, and re-reduction. The modest decrease in the extent of CO chemisorption by the catalyst after reaction is consistent with a slight decrease in the initial activity of the catalyst. Adsorption of CO on Ni(111) is favored at threefold hollow sites (*21*). Our observation that addition of Sn to Raney-Ni causes a decrease in the CO uptake is consistent with the report that adsorption of CO is strongly suppressed on a buckled $(\sqrt{3}x\ \sqrt{3})\ R30°$ Sn/Ni(111) surface, which has no threefold Ni hollow sites (*22*). The suppression of CO adsorption by addition of Sn to Ni may be analogous to the weakening of CO adsorption on Cu surfaces caused by Zn and ZnO species (*23*). The high CO:H ratio measured for our Raney-NiSn catalyst is also consistent with the adsorptive properties of NiSn alloys (*24*).

The beneficial effect of Sn on the selectivity for production of H_2 may be caused by the presence of Sn at Ni-defect sites and by the formation of Ni-Sn alloy surfaces, such as a Ni_3Sn alloy. For example, dissociation of CO leading to formation of methane over Ni catalysts may take place preferentially on Ni-defect sites (*25*), analogous to the preferential dissociation of dinitrogen on Ru-defect sites (*26*). The decoration of defect sites by Sn may thereby suppress methanation reactions, analogous to the observation that decoration of Ru-defect sites by Au decreases the sticking probability of N_2 at 500 K by seven orders of magnitude (*26*). It is also possible that methanation reactions are suppressed by the presence of Sn on Ni_3Sn alloy surfaces.

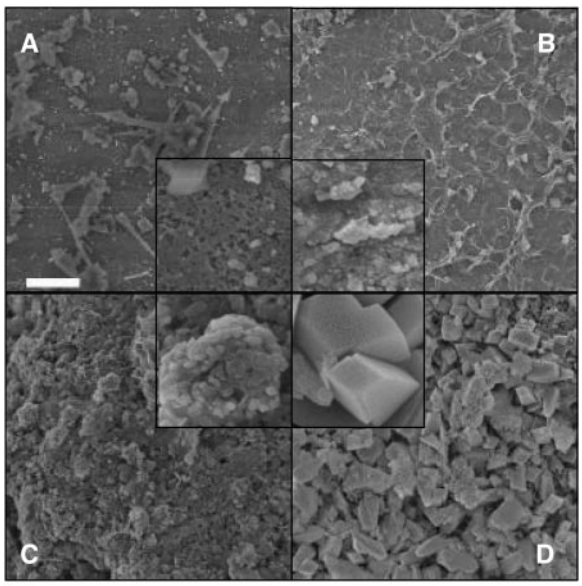

Fig. 2. SEM images of (**A**) Raney-Ni after reduction, (**B**) Raney-NiSn after reduction, (**C**) Raney-NiSn after reaction, Ni-rich phase, (**D**) Raney-NiSn after reaction, alumina-rich phase. Scale bar, 1.0 μm. Enlarged insets are magnified six times relative to main panels.

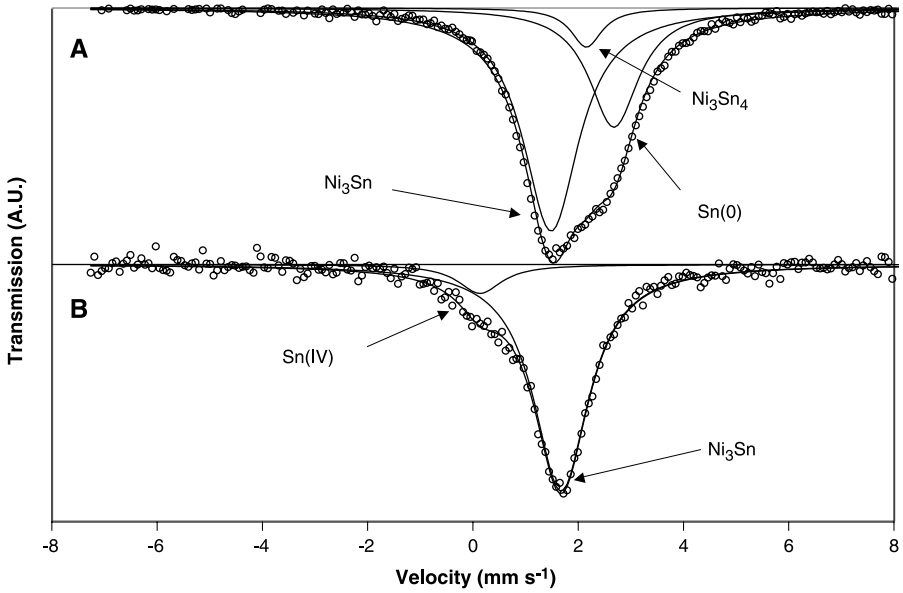

Fig. 3. In situ ^{119}Sn Mössbauer spectra of Raney-NiSn catalyst (**A**) after reduction at 533 K and (**B**) after reaction at 533 K and 51.4 bar with 5 wt % ethylene glycol feed for 60 hours.

References and Notes

1. J. Alper, *Science* **299**, 1686 (2003).
2. J. R. Rostrup-Nielsen, *Phys. Chem. Chem. Phys.* **3**, 283 (2001).
3. A. T. Bell, *Science* **299**, 1688 (2003).
4. D. R. Rolison, *Science* **299**, 1698 (2003).
5. D. J. Cole-Hamilton, *Science* **299**, 1702 (2003).
6. H. E. Schoemaker, D. Mink, M. G. Wubbolts, *Science* **299**, 1694 (2003).
7. R. D. Cortright, R. R. Davda, J. A. Dumesic, *Nature* **418**, 964 (2002).
8. R. R. Davda, J. W. Shabaker, G. W. Huber, R. D. Cortright, J. A. Dumesic, *Appl. Catal. B* **43**, 1 (2003).
9. J. W. Shabaker, R. R. Davda, G. W. Huber, R. D. Cortright, J. A. Dumesic, *J. Catal.* **215**, 344 (2003).
10. J. W. Shabaker, G. W. Huber, R. R. Davda, R. D. Cortright, J. A. Dumesic, *Catal. Lett.* **88**, 1 (2003).
11. P. Gallezot, N. Nicolaus, G. Fleche, P. Fuertes, A. Perrard, *J. Catal.* **180**, 51 (1998).
12. F. Ma, M. A. Hanna, *Bioresource Technol.* **70**, 1 (1999).
13. E. Tronconi *et al.*, *Chem. Eng. Sci.* **47**, 2451 (1992).
14. M. Mavrikakis, M. A. Barteau, *J. Mol. Catal. A: Chem.* **131**, 135 (1998).
15. J. F. E. Gootzen, W. Visscher, J. A. R. van Veen, *Langmuir* **12**, 5076 (1996).
16. J. F. E. Gootzen, A. H. Wonders, W. Visscher, J. A. R. van Veen, *Langmuir* **13**, 1659 (1997).
17. Materials and methods are available as supporting material on *Science* Online.
18. R. R. Davda, J. A. Dumesic, *Angew. Chem. Int. Ed.*, in press.
19. S. D. Robertson, J. Freel, R. B. Anderson, *J. Catal.* **24**, 130 (1972).
20. P. Nash, A. Nash, in *Binary Alloy Phase Diagrams*, T. B. Massalski, Ed. (ASM International, Materials Park, OH, ed. 2, 1992), vol. 3, pp. 2863–2864.
21. L. Becker *et al.*, *Phys. Rev. B* **47**, 9710 (1993).
22. C. Xu, B. E. Koel, *Surf. Sci.* **327**, 38 (1995).
23. J. Greeley *et al.*, *J. Catal.* **213**, 63 (2002).
24. M. Agnelli, J. P. Candy, J. M. Basset, J. P. Bournonville, O. A. Ferretti, *J. Catal.* **121**, 236 (1990).
25. H. P. Steinruck, M. P. D'evelyn, R. J. Madix, *Surf. Sci.* **172**, L561 (1986).
26. S. Dahl *et al.*, *Phys. Rev. Lett.* **83**, 1814 (1999).

27. Supported by the U.S. Department of Energy, Office of Basic Energy Sciences, Chemical Science Division, and by the National Science Foundation through a Small Business Technology Transfer grant and through the Materials Research Science and Engineering Center on Nanostructured Materials and Interfaces at the University of Wisconsin. We thank R. D. Cortright, C. Couto, R. R. Davda, and M. Mavrikakis for invaluable assistance.

Supporting Online Material

www.sciencemag.org/cgi/content/full/300/5628/2075/DC1
Materials and Methods
Figs. S1 to S3
Table S1

11 April 2003; accepted 29 May 2003